

Combining single-cell RNA sequencing with spatial transcriptome analysis reveals dynamic molecular maps of cambium differentiation in the primary and secondary growth of trees

Renhui Li^{1,2}, Zhifeng Wang¹, Jia-Wei Wang^{1,3} and Laigeng Li^{1,*}

¹National Key Laboratory of Plant Molecular Genetics and CAS Center for Excellence in Molecular Plant Sciences, Institute of Plant Physiology and Ecology, Chinese Academy of Sciences, Shanghai 200032, China

²University of the Chinese Academy of Sciences, Beijing 100049, China

³School of Life Science and Technology, ShanghaiTech University, Shanghai 201210, China

*Correspondence: Laigeng Li (ligli@cemps.ac.cn)

<https://doi.org/10.1016/j.xplc.2023.100665>

ABSTRACT

Primary and secondary growth of the tree stem are responsible for corresponding increases in trunk height and diameter. However, our molecular understanding of the biological processes that underlie these two types of growth is incomplete. In this study, we used single-cell RNA sequencing and spatial transcriptome sequencing to reveal the transcriptional landscapes of primary and secondary growth tissues in the *Populus* stem. Comparison between the cell atlas and differentiation trajectory of primary and secondary growth revealed different regulatory networks involved in cell differentiation from cambium to xylem precursors and phloem precursors. These regulatory networks may be controlled by auxin accumulation and distribution. Analysis of cell differentiation trajectories suggested that vessel and fiber development followed a sequential pattern of progressive transcriptional regulation. This research provides new insights into the processes of cell identity and differentiation that occur throughout primary and secondary growth of tree stems, increasing our understanding of the cellular differentiation dynamics that occur during stem growth in trees.

Key words: scRNA-seq, spatial transcriptome, primary growth, secondary growth, secondary cell wall, SCW, *Populus*

Li R., Wang Z., Wang J.-W., and Li L. (2023). Combining single-cell RNA sequencing with spatial transcriptome analysis reveals dynamic molecular maps of cambium differentiation in the primary and secondary growth of trees. *Plant Comm.* **4**, 100665.

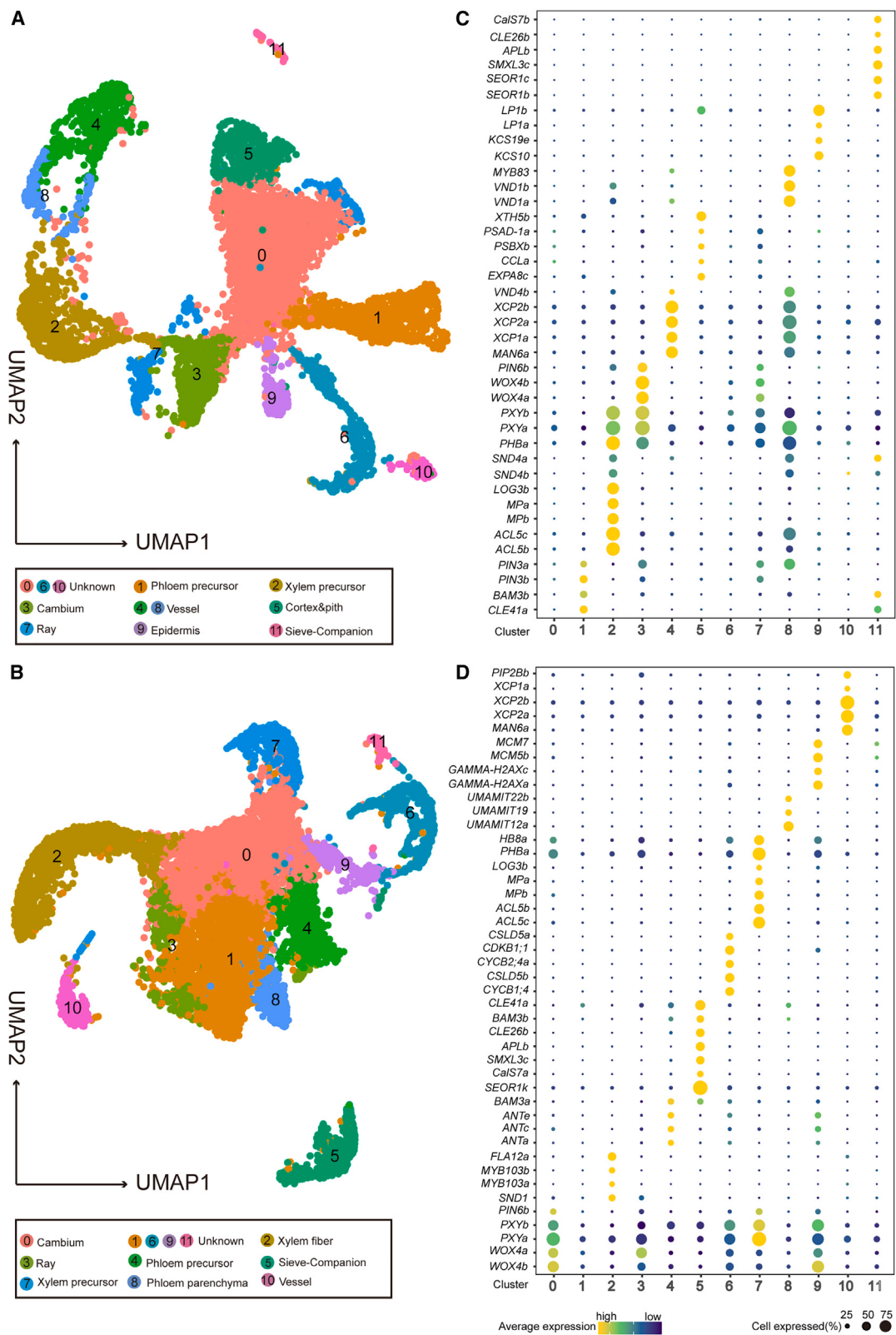
INTRODUCTION

Primary growth occurs at the shoot apical meristem through divisions that begin in the procambium and give rise to primary vascular bundles. Secondary growth depends on periclinal divisions in the vascular cambium that produce secondary xylem and phloem (Larson, 2012; Zhu et al., 2018; Luo and Li, 2022). Although both cambiums share some biological properties, cell division and differentiation in the vascular cambium during secondary growth differ from those in the apical meristem (Baucher et al., 2007; Carlquist, 2013). The secondary xylem, often known as wood, is a key pool for the assimilation of the majority of photosynthetic carbon products, which are renewable and required by humans (Pan et al., 2011). Understanding wood formation has thus attracted significant

attention, as wood is critical for carbon storage and production of sustainable green materials.

The cellular structure and organization of wood derived from proliferation of the vascular cambium have been described in the literature (Larson, 2012). The vascular cambium is thought to be a zone of dividing cells that contains cambial initials (stem cells) and phloem or xylem precursors (Esau, 1977; Bossinger and Spokevicius, 2018). Cambium zone cells are typically distinguished by their undifferentiated state and smaller size compared with neighboring cells. Cambium cell division and

Published by the Plant Communications Shanghai Editorial Office in association with Cell Press, an imprint of Elsevier Inc., on behalf of CSPB and CEMPS, CAS.

**Figure 1. Identification of cell clusters from the primary growth stem and secondary growth stem.**

(A) UMAP representation of 12 PGT clusters. Each dot corresponds to a single cell. Cell clusters are labeled with numbers and different colors. PGT stands for primary growth tissue.

(legend continued on next page)

subsequent cell differentiation have been investigated in the model plant *Arabidopsis* (Niemenen et al., 2015). Studies have revealed that a local maximum of the phytohormone auxin in the *Arabidopsis* root contributes to specification of a stem cell organizer for cambium meristem activity (Zhang et al., 2019). By increasing cytokinin biosynthesis, overexpression of *AHL15* changes herbaceous *Arabidopsis* into a plant with secondary growth. This finding suggests that constant cytokinin biosynthesis may be needed for secondary growth based on cambium division (Rahimi et al., 2022). However, the identity and differentiation pathways of cambial cells in woody plants have not been fully established owing to a lack of sufficient molecular markers. Wood formation is linked to complex transcriptional programs that regulate cambium cell activity, xylem differentiation, and secondary cell wall (SCW) biosynthesis (Baucher et al., 2007; Luo and Li, 2022). However, owing to technical difficulties in monitoring molecular activities at the cellular level during tree stem growth, studies of wood formation have primarily concentrated on tissue-level transcriptional activities and reverse genetics. It remains to be seen how transcriptional activities in tree secondary growth can be resolved dynamically and sequentially at the cellular level. Single-cell RNA sequencing (scRNA-seq) has recently revolutionized our understanding of gene expression in individual cells. The use of scRNA-seq methods to analyze wood-forming tissue at a single-cell resolution led to identification of heterogeneous cell transcriptomes that could be classified into different cell clusters (Chen et al., 2021; Li et al., 2021; Tung et al., 2023). scRNA-seq of protoplasts prepared from differentiating xylem of *Populus* revealed that the xylem tissue was divided into 12 cell clusters (Li et al., 2021). Another study identified 20 cell clusters using RNA-seq of protoplasts from highly lignified poplar stems (Chen et al., 2021). Because of the various parameters used to identify cell clusters, the same tissue can be divided into different numbers of clusters. Cell-cluster identification is based primarily on the reduction of linear dimensionality via principal-component analysis (PCA) of cell transcriptomes obtained from single-cell samples. Tissues are organized from various cell types with varying developmental statuses, and the dimensional complexity of cell transcriptomes is influenced by both cell type and developmental state. It is therefore challenging to precisely map cell types and dynamic cell status through scRNA-seq data processing. In this study, we constructed a cell atlas of primary growth tissue (PGT) and secondary growth tissue (SGT) from the *Populus* stem. Because these tissues show both similarities and differences in many aspects of cell identification and differentiation, comparison of their cell atlases and differentiation trajectories provided cross-verification of cell-cluster identification and cell development. The combination of scRNA-seq analysis and spatial transcriptome information aided in validation of the cell atlas and spatial differentiation. The results of this combined approach provide new insights into the cellular atlas and differentiation of tree stem growth.

RESULTS

Single-cell transcriptome analysis of *Populus* tissues undergoing primary and secondary growth

Primary growth of the tree stem depends on the shoot apical meristem, whereas secondary growth results from proliferation of the vascular cambium (Prassinos et al., 2005; Zhu et al., 2018). We harvested the first to third internodes of the *Populus* stem tip, which contain PGT (supplemental Figure 1A–1C), and the fifth to tenth internodes of the stem, which contain SGT (supplemental Figure 1A and 1E–1G), in order to examine transcriptomic activities of the two growth processes at single-cell resolution. Protoplasts were prepared according to an optimized procedure (Lin et al., 2014), and high-purity, viable protoplasts were separated from the stem tissues. The 10x Genomics Next GEM Single Cell Kit was used to create scRNA-seq libraries, which were then sequenced on the Illumina NovaSeq 6000 platform. After cell- and gene-level filtration, we recovered 7416 PGT cells and 11 769 SGT cells, which showed expression of about 27 000 and 29 317 genes, respectively (supplemental Table 1). After linear dimensional reduction, we used the Clustree package to examine dynamic changes in clusters under various resolution parameters. We looked at the total number of clusters, the number of clusters that merged into one, and the number of clusters that split into different clusters to determine the best resolution parameter for cluster identification. Optimized resolution parameters were used to ensure that the cell types were correctly clustered together and visualized by Uniform Manifold Approximation and Projection (UMAP) (Becht et al., 2018). The analysis revealed 12 cell clusters in each of the two tissues (Figure 1A and 1B). Genes that were specifically expressed in one or two clusters were identified as cluster-enriched genes (supplemental Tables 2 and 3). We examined the expression of marker genes in distinct clusters to identify the detected clusters with the correct cell type (Figure 1C and 1D). The marker genes included the cambium cell markers *WUSCHEL-RELATED HOMEOBOX 4* (*WOX4*) and *PHLOEM INTERCALATED WITH XYLEM* (*PXY*) (Suer et al., 2011); the xylem precursor markers *ACAULIS 5* (*ACL5*), *LONELY GUY 3* (*LOG3*), *AUXIN RESPONSE FACTOR 5* (*MP*), and *PHABULOSA* (*PHB*) (Clay and Nelson, 2005; Prigge et al., 2005; Vidaurre et al., 2007; Kuroha et al., 2009); the phloem precursor markers *AINTEGUMENTA* (*ANT*) and *BETA-AMYLASE 3* (*BAM3*) (Rodriguez-Villalon et al., 2014); the xylem fiber markers *SECONDARY WALL-ASSOCIATED NAC DOMAIN 1* (*SND1*) and *MYB DOMAIN PROTEIN 103* (*MYB103*) (Zhong et al., 2006, 2008); the vessel markers *XYLEM CYSTEINE PEPTIDASE 1* (*XCP1*), *XCP2*, *ENDO-BETA-MANNASE 6* (*MAN6*), and *VASCULAR-RELATED NAC-DOMAIN PROTEIN 1* (*VND1*) (Funk et al., 2002; Avci et al., 2008; Zhao et al., 2013; Zhou et al., 2014); the sieve markers *CALLOSE SYNTHASE 7* (*Cals7*), *ALTERED PHLOEM DEVELOPMENT* (*APL*), and *SIEVE-ELEMENT-OCLUSION-RELATED 1* (*SEOR1*) (Bonke et al.,

(B) UMAP representation of 12 SGT clusters. Each dot corresponds to a single cell. Cell clusters are labeled with numbers and different colors. SGT stands for secondary growth tissue.

(C) Expression profiles of representative marker genes in each PGT cluster. The size of the dot indicates the percentage of cluster cells that express a given gene. Color indicates the average expression level.

(D) Expression profiles of representative marker genes in each SGT cluster. The size of the dot indicates the percentage of cluster cells that express a given gene. Color indicates the average expression level.

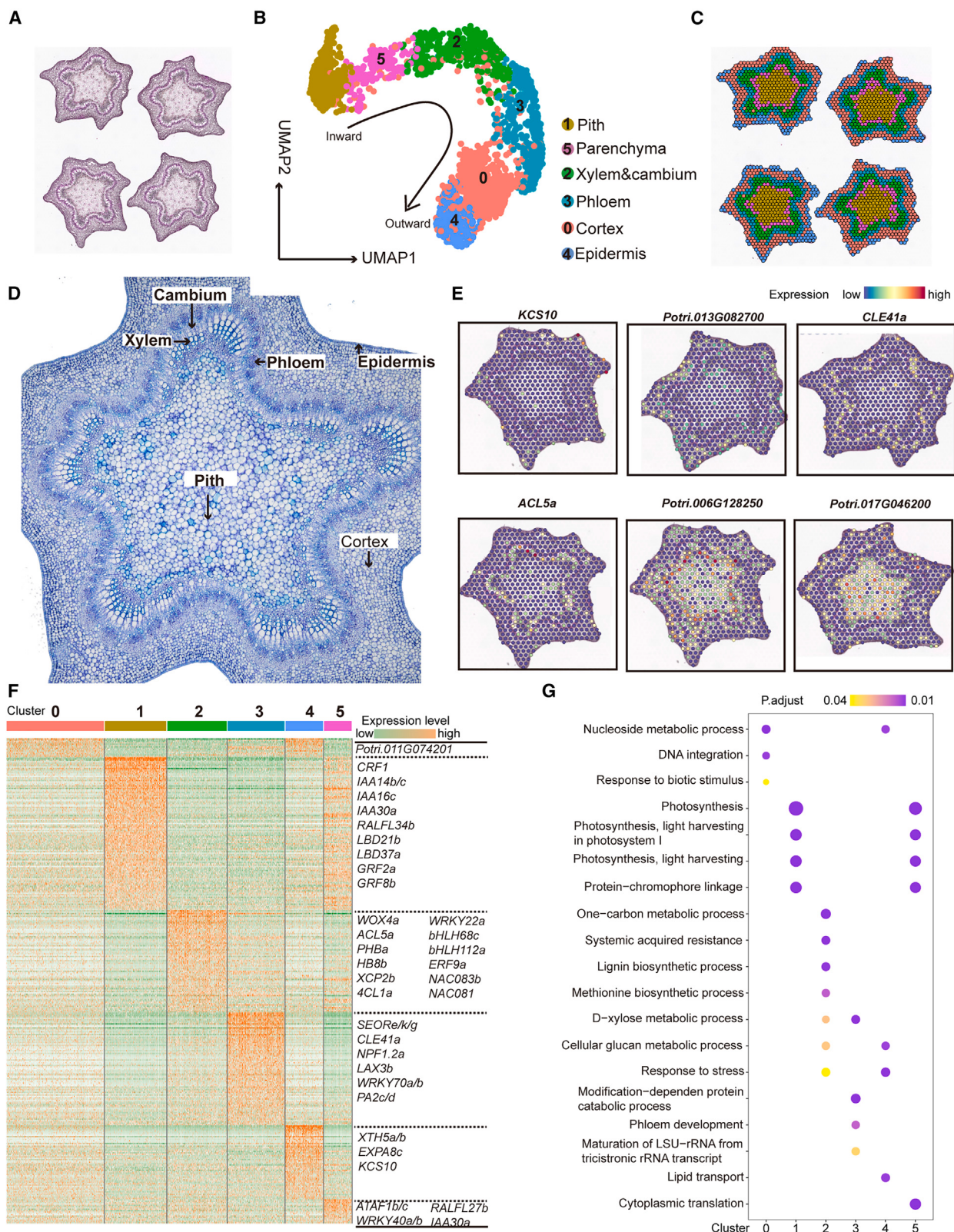


Figure 2. Reconstruction of the cellular organization of the *Populus* stem based on spatial transcriptomics.

(A) Frozen sections of *Populus* stem were stained with hematoxylin and eosin.

(B) UMAP display of cell clusters identified by spatial transcriptomics. Different colors represent cell clusters.

(C) Cell clusters mapped over images of sections stained with hematoxylin and eosin. Cell clusters are colored as in (B).

(legend continued on next page)

2003; Pelissier et al., 2008; Barratt et al., 2011; Xie et al., 2011); and the phloem parenchyma markers *USUALLY MULTIPLE ACIDS MOVE IN AND OUT TRANSPORTERS 12* (*UMAMIT12*), *UMAMIT19*, and *UMAMIT22* (Kim et al., 2021). In addition, spatial transcriptomics analysis revealed that expression of *3-KETOACYL-COA SYNTHASE 10* (*KCS10*) was mapped to the epidermis and that of *CCR-LIKE* (*CCL*) and *PHOTOSYSTEM II SUBUNIT X* (*PSBX*) was mapped to the cortex and pith (supplemental Table 4). Cell-type assignment for cluster identification was studied further using GO pathway analysis. Expression of genes in the secondary cell wall biogenesis pathway was significantly concentrated in fiber and vessel cell clusters, whereas phloem development genes were expressed in sieve companion cells (supplemental Figure 1H). The analysis led to identification of 12 cell clusters in PGT. Nine clusters were identified as cambium, xylem precursor, phloem precursor, sieve, vessel, epidermis, ray parenchyma, cortex, and pith cells. Cluster 5 contained two cell types: cortex and pith. Both clusters 4 and 8 contained vessel cells, but cluster 4 represented early-stage cells and cluster 8 represented late-stage cells (Figure 1A and 1B). However, clusters 0, 6, and 10 in PGT did not have a particular cell type assigned to them (Figure 1A). Twelve cell clusters were also identified in SGT. Eight were assigned to specific cell types: cambium, xylem precursor, phloem precursor, sieve, phloem parenchyma, vessel, fiber, and ray parenchyma (Figure 1B). Genes related to mitosis and the cell cycle were highly expressed in clusters 6 and 9, indicating that these clusters contained a high density of dividing cells. Clusters 1, 6, 9, and 11 were not assigned to a specific cell type (Figure 1B).

Spatial transcriptome sequencing of the *Populus* stem

We performed spatial transcriptome sequencing of the *Populus* stem to characterize cell transcriptomes in cross-sections of growing stem tissue. The stem was frozen and sectioned for spatial sequencing on the 10x Genomics Visium platform (Figure 2A). After filtration, we obtained 2406 spots, with a median of 1962 genes sequenced for each spot, covering transcription of a total of 23 886 genes (supplemental Table 1). The spots were divided into six clusters (Figure 2B) after linear regression and UMAP visualization of the spatial transcriptomes. The sequenced spots were mapped to the corresponding regions of the stem cross-section (Figure 2C) and were assigned to the pith, parenchyma, xylem and cambium, phloem, cortex, and epidermis (Figure 2B–2D). Expression of cell-type marker genes in the six clusters corresponded to their locations in the cross-section (Figure 2E). Specific cell types were considerably enriched in their corresponding marker genes: the vessel markers *XCP1* and *XCP2*, the xylem precursor marker *ACL5*, the cambium marker *WOX4*, and the phloem markers *SEOR1* and *CLAVATA3/ESR-RELATED 41* (*CLE41*) (Figure 2F). GO pathway analysis revealed that the majority of lipid transport genes, lignin biosynthesis genes, and phloem development genes were

expressed in the epidermis, xylem, and phloem, respectively (Figure 2G). The results showed a high degree of consistency among the anatomical regions of gene expression, the cell type identifications, and the single-cell transcriptomes.

Cambium identity

Cambium is a type of cell that is essential for the growth and development of tree stems, and *WOX4* and *PXY* are considered to be cambium cell markers. *PXY* expression was found in four PGT clusters (xylem precursors, early vessel cells, cluster 3, and cluster 7) (Figure 1C), and *WOX4* expression was found in clusters 3 and 7. *PXY* and *WOX4* expression was also found in five SGT clusters (cell cycle clusters 6 and 9, xylem precursor cells, and clusters 0 and 3) (Figure 1D). The cambium markers *WOX4* and *PXY* were thus expressed in more than one cluster. Although the resolution parameter has an effect on the number of clusters created, clustering with different resolution settings had no effect on the expression of *PXY* and *WOX4* in multiple cell clusters (Figure 3A). To validate this result, we examined *PXY* and *WOX4* expression in other studies and found that they were likewise expressed in various clusters (supplemental Figure 2A). The highly enriched genes in the four clusters expressing *PXY* and *WOX4* were then used for GO pathway analysis. The clusters PC3 and SC0 were enriched in the phloem and xylem histogenesis pathway, whereas PC7 and SC3 were enriched in three stress-response pathways: response to heat, response to hydrogen peroxide, and response to reactive oxygen species (Figure 3B). *In situ* hybridization was performed to identify the cell types that expressed the stress-response pathway genes (Figure 3C–3E). Specific genes from the PC7 and SC3 clusters were expressed in early ray parenchyma cells, whereas specific genes from PC3 and SC0 were expressed in cambium (Figure 3E). We also examined how the cluster genes were expressed by comparing them with microdissection gene expression data from xylem, phloem, cambium, and other cell types (Dai et al., 2023; Tung et al., 2023). The PC3 and SC0 cluster genes were matched to cambium (supplemental Figure 2B and 2C), and the genes in the PC7 and SC3 clusters were found to be associated with fiber, vessel, and ray cells (supplemental Figure 2D and 2E). *WOX4* and *PXY* were also matched to ray cells (supplemental Figure 2F). Thus, PC3 and SC0 were assumed to be cambium initials for xylem and phloem cells, but PC7 and SC3 were assumed to be ray initial cells. Because ray cells express *WOX4* and *PXY*, as well as stress-response pathway genes, it would be worthwhile to determine the role played by these cells during stem secondary growth.

Trajectory of xylem and phloem differentiation from cambium

Differentiation of the procambium during primary growth and the vascular cambium during secondary growth into xylem and phloem results in development of the vascular structure.

(D) Paraffin-embedded sections of *Populus* stem stained with toluidine blue.

(E) Spatial expression pattern of marker genes. The color bar indicates the expression level.

(F) Expression heatmap of significantly enriched genes in each cluster. Representative marker genes are listed on the right. Colors reflect the expression level.

(G) GO enrichment of highly enriched genes in each cluster. The size of the dot represents the number of genes, and the color denotes the adjusted *P* value in the related pathway.

Plant Communications

Molecular maps of cambium differentiation

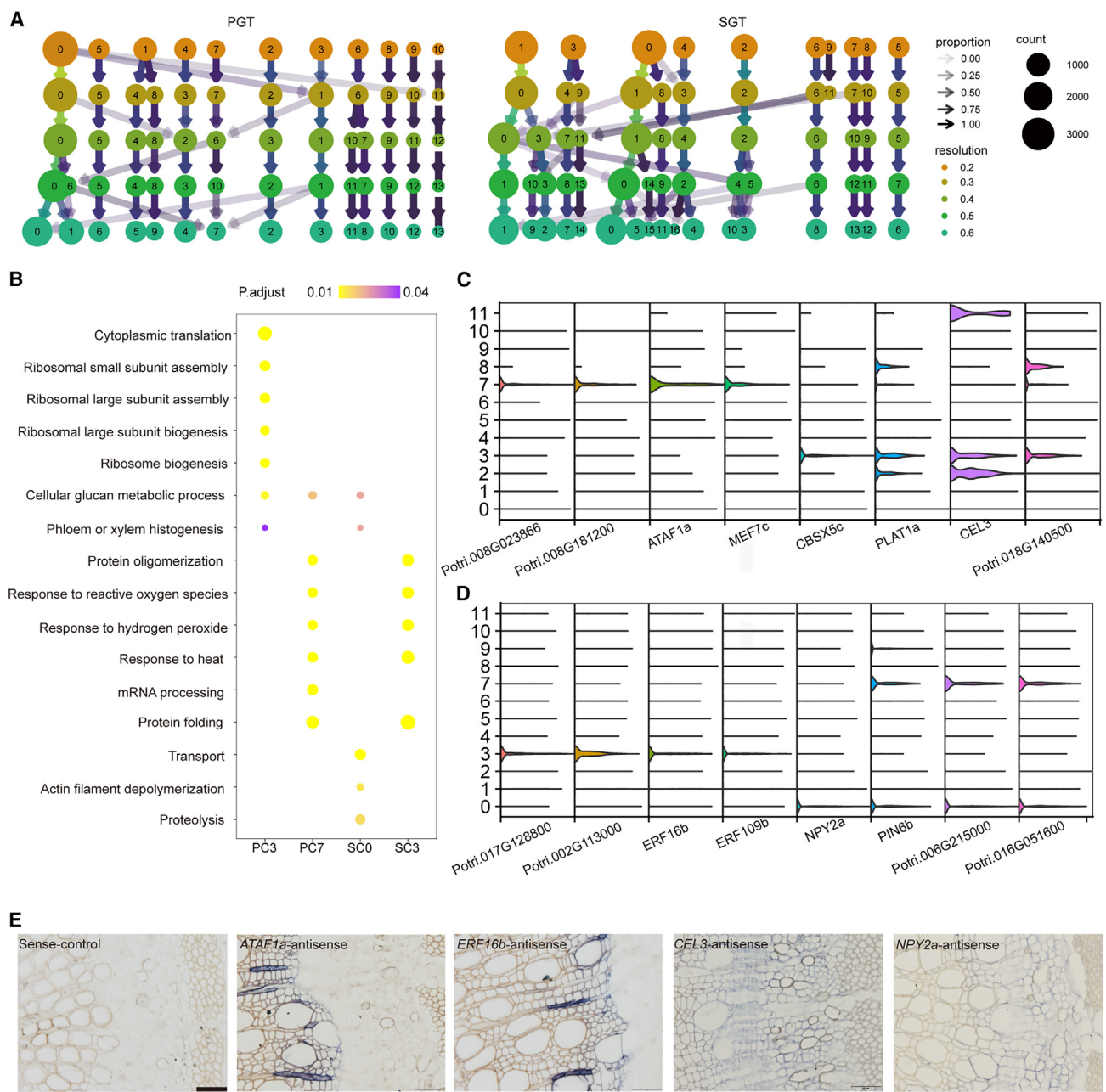


Figure 3. Identification of cambium.

(A) Clustree of clustering in Seurat at various resolution settings. The size of the circle represents the number of cells in each cluster. The color of the circle shows the resolution setting. The transparency of the arrows represents the change in proportion between clusters with different resolution settings. In this study, a resolution setting of 0.3 was selected. PGT is on the left and SGT on the right.

(B) GO enrichment of the highly enriched genes in four clusters (PC3, cluster 3 in PGT; PC7, cluster 7 in PGT; SC0, cluster 0 in SGT; SC3, cluster 3 in SGT). The size of the dot represents the number of genes, and the color denotes the adjusted P value in the related pathway.

(C) Violin plots showing expression levels of PC7 cluster genes (*Potri.008G023866*, *Potri.008G181200*, *ATAF1a*, and *MEF7c*) and PC3 cluster genes (*CBSX5c*, *PLAT1a*, *CEL3*, and *Potri.018G140500*).

(D) Violin plots showing the expression levels of SC0 cluster genes (*Potri.017G128800*, *Potri.002G113000*, *ERF16b*, and *ERF109b*) and SC3 cluster genes (*NPY2a*, *PIN6b*, *Potri.006G215000*, and *Potri.016G051600*).

(E) RNA *in situ* hybridization. Scale bars correspond to 50 μm. *ATAF1a* expression in PC7, *ERF16b* expression in SC3, *CEL3* expression in PC3, and *NPY2a* expression in SC0 are shown.

Pseudo-time analysis was performed to arrange cells with comparable developmental transcriptomes in order and thus examine the trajectory of cambium differentiation in PGT and SGT. To construct pseudo-time trajectories, we first collected cambium,

xylem precursor, and phloem precursor cell clusters from PGT and SGT. As shown in Figure 4A, cambium cells, xylem precursors, and phloem precursors were built sequentially, with cambium serving as the starting point and xylem and phloem

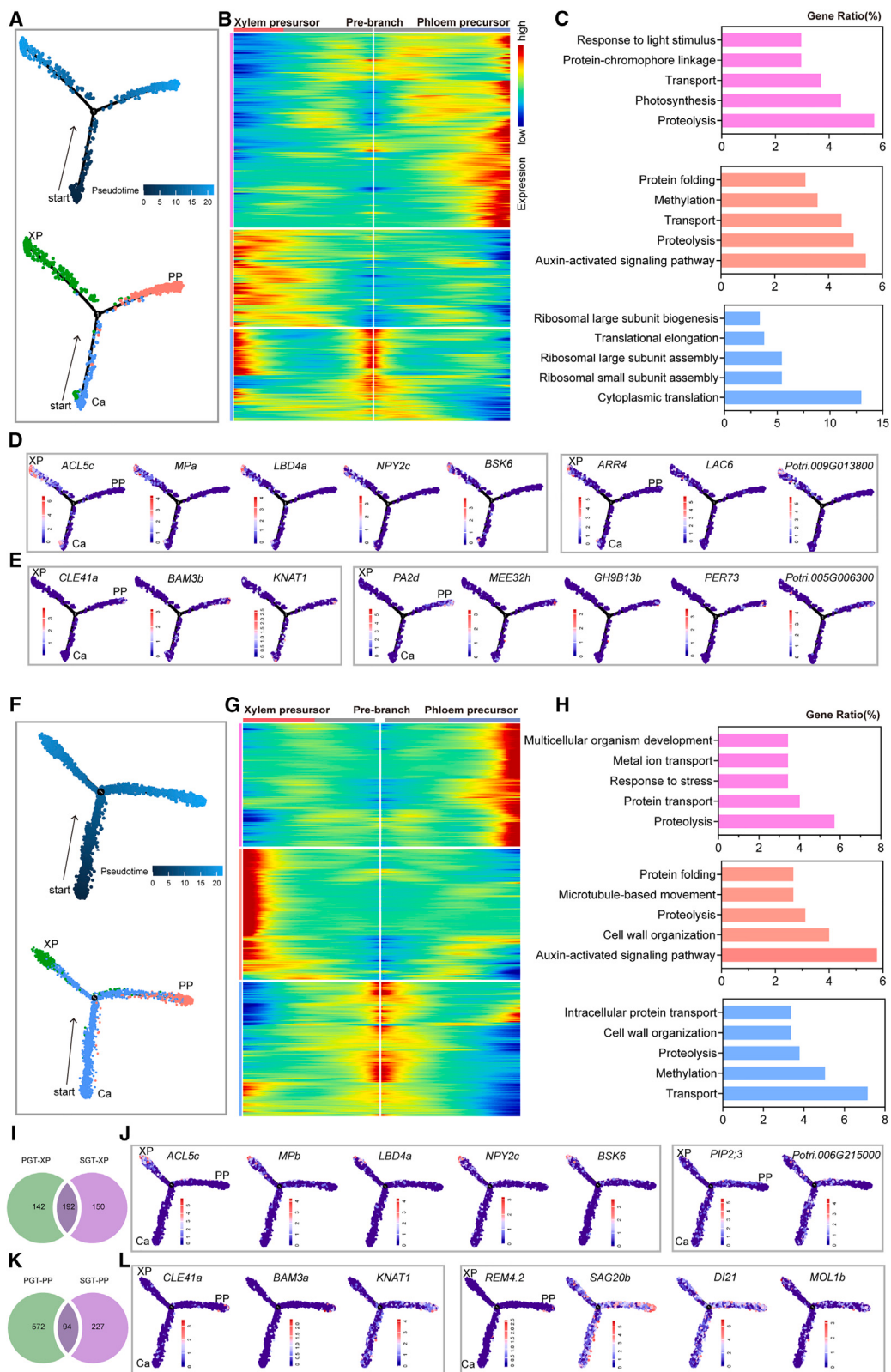


Figure 4. Trajectories of cambium differentiation toward xylem and phloem precursors in PGT and SGT.

(A) Pseudo-time trajectory of cambium differentiation in PGT. The pseudo-time of the trajectory (above) and cell-type differentiation (Ca, cambium; XP, xylem precursor; PP, phloem precursor) in the trajectory (below) are shown. Each dot represents a cell.

(legend continued on next page)

precursors differentiating into two branches in PGT. The trajectories were mapped by computing gene changes to arrange the cells in an ordered sequence. Branch-dependent genes whose expression was related to cell differentiation into xylem or phloem precursors in PGT were mapped (Figure 4B). The expression of branch-dependent genes showed three patterns: increased expression in phloem precursors, increased expression in xylem precursors, or high expression in cambium followed by decreasing expression during differentiation. Enriched GO pathways in these genes are listed in Figure 4C. The xylem branch-dependent genes included xylem precursor marker genes. For example, expression of *ACL5*, which controls *Arabidopsis* xylem specification, and *MP*, which encodes a major auxin response transcription factor in xylem (Muñiz et al., 2008), increased steadily toward the xylem precursor branch (Figure 4D). Homologs of *LOB DOMAIN-CONTAINING PROTEIN 4 (LBD4)*, *NAKED PINS IN YUC MUTANTS 2 (NPY2)*, and *BRASSINOSTEROID-SIGNALING KINASE 6 (BSK6)* were also strongly expressed in the xylem precursor branch (Figure 4D). Another study (supplemental Figure 3A) also showed that these genes were involved in xylem cell development (Chen et al., 2021). Homologs of *ARABIDOPSIS RESPONSE REGULATOR 4 (ARR4)*, a negative regulator of cytokinin signaling (To et al., 2007), and *LACCASE 6 (LAC6)* were discovered in the xylem precursor branch of PGT (Figure 4D). By contrast, these genes were rarely expressed in the SGT trajectory (supplemental Figure 3B). Tissue transcriptome sequencing revealed that these genes were considerably more abundant in PGT than in SGT (supplemental Figure 3C and supplemental Table 5). This suggested that these genes have a role in PGT xylem differentiation. As cells moved toward the phloem precursor branch, the phloem precursor markers *CLE41*, which encodes the TDIF peptide for control of cambium proliferation (To et al., 2007), and *BAM3*, a receptor kinase (Depuydt et al., 2013), gradually increased in expression (Figure 4E). *KNOTTED-LIKE HOMEOBOX OF ARABIDOPSIS THALIANA 1 (KNAT1)*, *PA2*, *MEE32*, *GH9B13*, and *PER73* were also phloem precursor branch-dependent genes (Figure 4E). Surprisingly, these genes showed almost no expression in SGT (supplemental Figure 3D), but tissue RNA-seq showed that they were highly expressed in PGT (supplemental Figure 3E). The

trajectory of cambium differentiation in SGT revealed the differentiation path of xylem and phloem precursor cells from cambium (Figure 4F). Figure 4G shows the mapping of the branch-dependent genes whose expression was linked to cell differentiation into xylem or phloem precursors in SGT. As in PGT, the expression of branch-dependent genes in SGT showed three patterns: increased expression in phloem precursors, increased expression in xylem precursors, and high expression in the cambium followed by decreasing expression during differentiation. GO analysis suggested the likely biological processes involved (Figure 4H). We next compared xylem precursor branch genes in PGT with those in SGT and discovered that more than half of them overlapped, including *ACL5*, *MP*, *LBD4*, *NPY2*, and *PSBK6* (Figure 4I and 4J). However, homologs of *PLASMA MEMBRANE INTRINSIC PROTEIN 2;3 (PIP2;3)* and several genes of unknown function were significantly expressed in SGT but not in PGT (Figure 4J; supplemental Figure 3F and 3G). *CLE41*, *BAM3*, and *KNAT1* were strongly expressed in phloem precursor branches of both PGT and SGT (Figure 4K and 4L). Expression of *REMORIN GROUP 4.2 (REM4.2)*, *SENESCENCE-ASSOCIATED GENE 20 (SAG20)*, *DROUGHT-INDUCED 21 (DI21)*, and *MORE LATERAL GROWTH1 (MOL1)* was high in SGT but low in PGT (Figure 4L; supplemental Figure 3H). Tissue transcriptome sequencing confirmed this disparity (supplemental Figure 3I). These findings imply that these genes have a role in the differentiation of phloem precursor cells in SGT. We also compared the expression of branch-dependent genes with previously published data (Chen et al., 2021). The appropriate cell type was assigned to 153 xylem precursor branch genes and 125 phloem precursor branch genes (supplemental Tables 6 and 7). For example, *HB8*, *PHB*, and *LBD4* and the auxin-related genes *ACL5*, *MP*, *LIKE AUXIN-RESISTANT 2 (LAX2)*, *INDOLE-3-ACETIC ACID INDUCIBLE 9 (IAA9)*, *IAA11*, *IAA13*, and *IAA19*, which reflect the auxin activation signaling pathway, were enriched in xylem precursors (Figure 4C and 4H; supplemental Table 6), whereas *ANT*, *SMAX1-LIKE 5 (SMXL5)*, and *AINTEGUMENTA-LIKE 5 (AIL5)* were expressed in phloem precursors in previously published data (supplemental Table 7) (Chen et al., 2021). In summary, xylem and phloem differentiation in PGT and SGT involves both shared molecular networks and PGT- and SGT-specific

- (B)** Heatmap depicting the expression dynamics of branch-dependent genes in PGT along the differentiation trajectory toward xylem and phloem precursors on two sides. The branch-dependent genes show three differentiation patterns.
- (C)** Bar chart of GO enrichment of branch-dependent genes. The top 5 pathways were identified for the three differentiation patterns in **(B)**.
- (D)** Expression of xylem precursor branch genes along the differentiation trajectory in PGT. Each dot represents a cell. The color bar indicates the expression level.
- (E)** Expression of phloem precursor branch genes along the differentiation trajectory in PGT. Each dot represents a cell. The color bar indicates the expression level.
- (F)** Pseudo-time trajectory of cambium differentiation in SGT. The pseudo-time of the trajectory (above) and cell-type differentiation (Ca, cambium; XP, xylem precursor; PP, phloem precursor) in the trajectory (below) are shown. Each dot represents a cell.
- (G)** Heatmap depicting the expression dynamics of branch-dependent genes in SGT along the differentiation trajectory toward xylem and phloem precursors on two sides. The branch-dependent genes show three differentiation patterns.
- (H)** Bar chart of GO enrichment of branch-dependent genes. The top 5 pathways were identified for the three differentiation patterns in **(G)**.
- (I)** Venn diagram showing numbers of shared and phase-specific expressed genes for xylem precursor branch genes. Green indicates genes in PGT, and purple indicates genes in SGT.
- (J)** Expression of xylem precursor branch genes along the differentiation trajectory in SGT. Each dot represents a cell. The color bar indicates the expression level.
- (K)** Venn diagram showing numbers of shared and phase-specific expressed genes for phloem precursor branch genes. Green indicates genes in PGT, and purple indicates genes in SGT.
- (L)** Expression of phloem precursor branch genes along the differentiation trajectory in SGT. Each dot represents a cell. The color bar indicates the expression level.

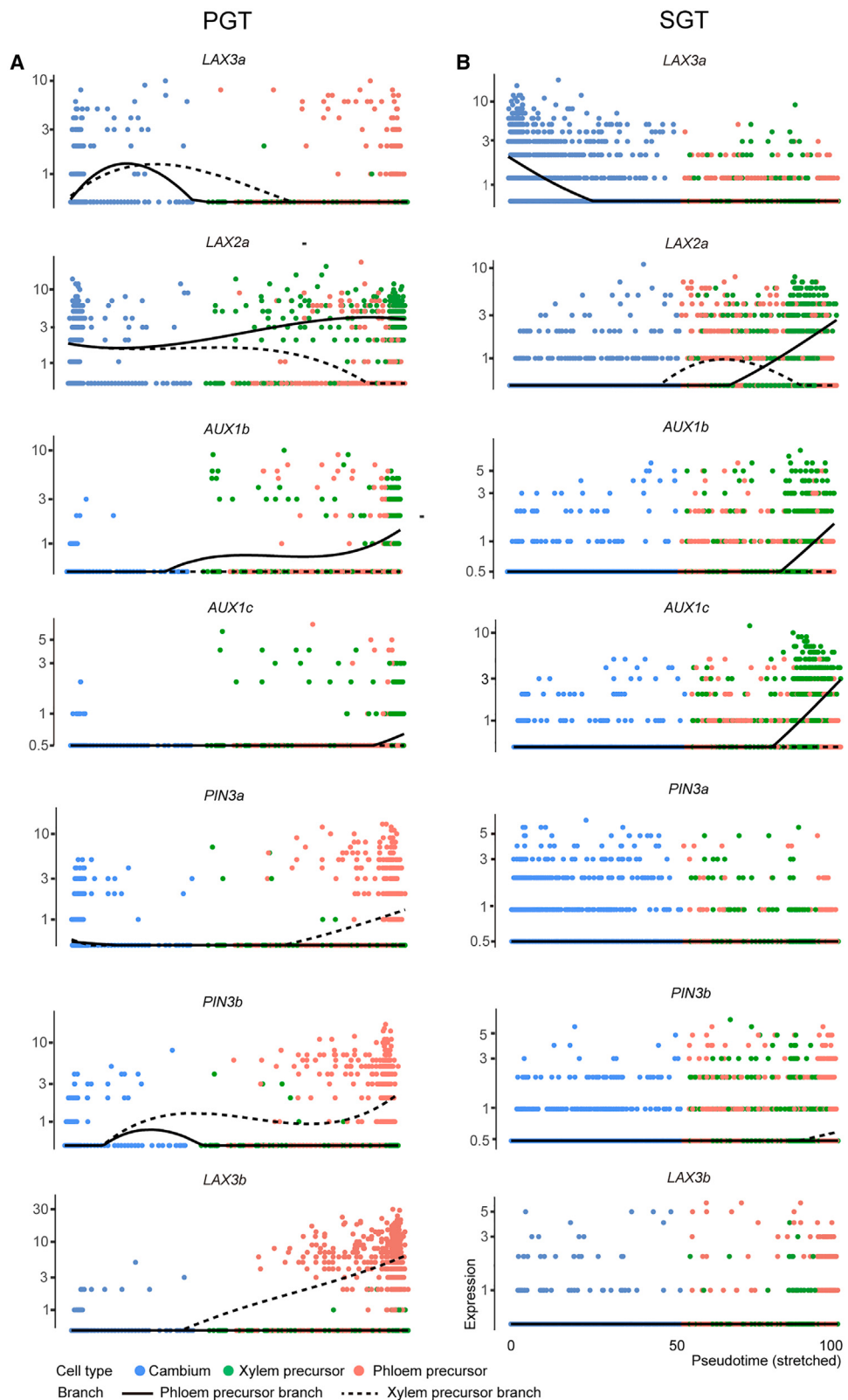
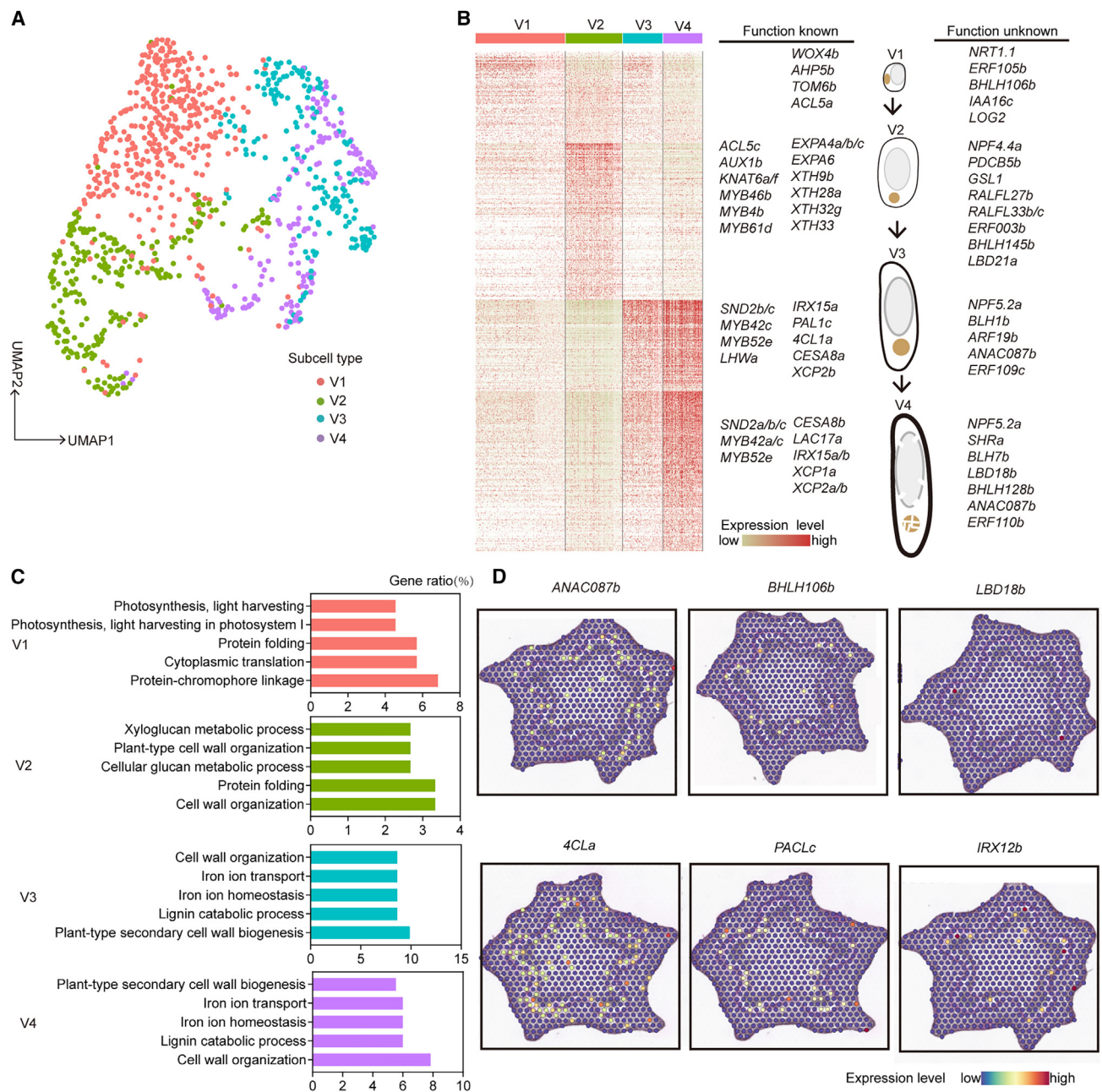


Figure 5. Dynamics of auxin transporter expression in PGT and SGT through the cambium differentiation trajectory.

(A) Auxin transporter expression dynamics over the differentiation trajectory in PGT. A dot represents a cell, and the colors denote the cell-type cluster. (B) Auxin transporter expression dynamics over the differentiation trajectory in SGT. A dot represents a cell, and the colors denote the cell-type cluster. The solid line indicates the phloem precursor branch, and the dotted line indicates the xylem precursor branch.

**Figure 6. Vessel development analysis.**

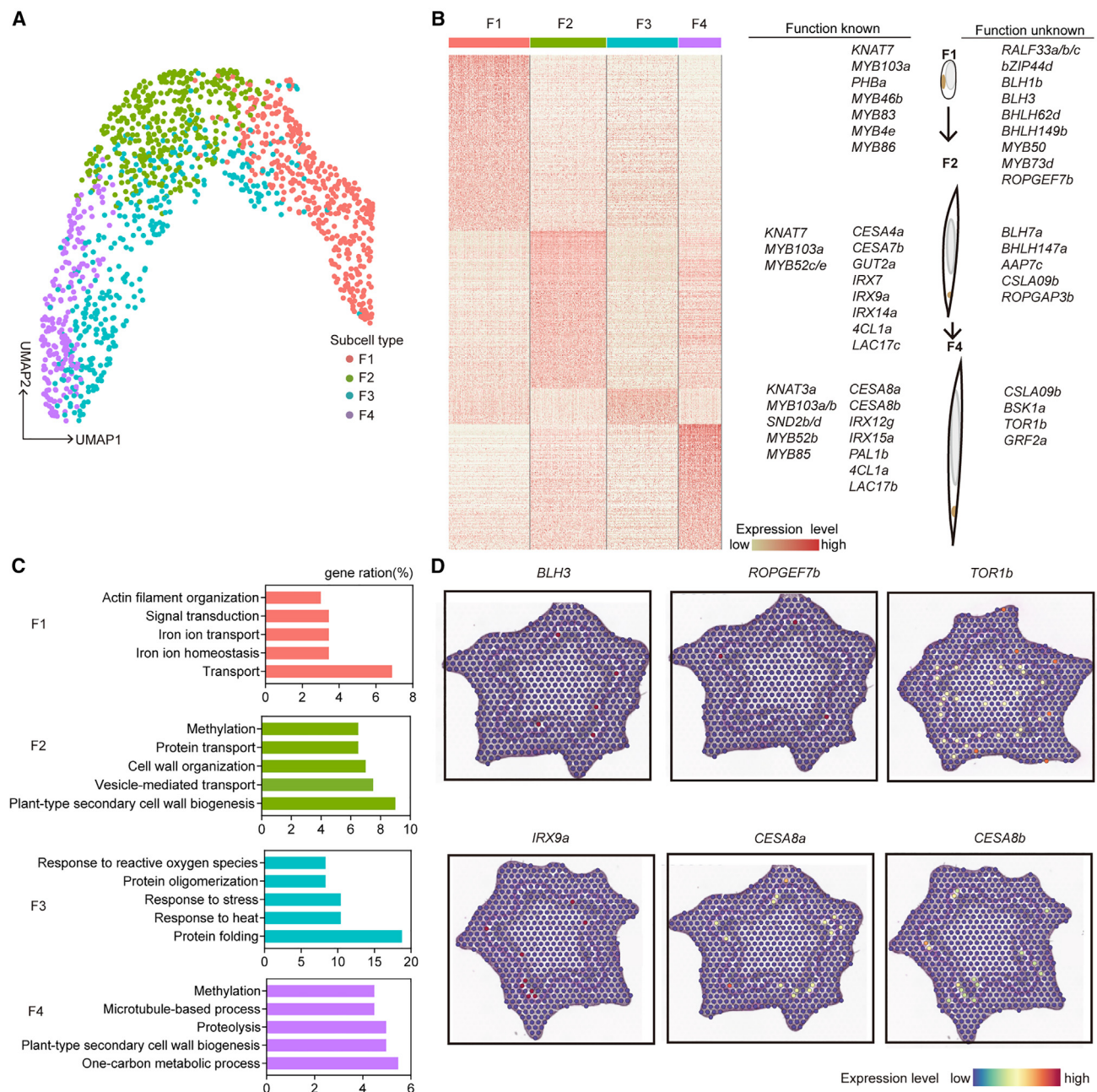
- (A) UMAP analysis showing that the vessel cell cluster is separated into four subgroups. The subgroups are color coded.
- (B) Heatmap depicting the highly enriched genes in each vessel subgroup. Two columns list representative genes. Genes with known and unknown functions in vessel development are listed separately. The color of the dots indicates the expression level.
- (C) GO enrichment of the most enriched genes in each vessel subgroup.
- (D) Spatial expression pattern of vessel-enriched genes in the stem cross-section. The color of the dots indicates the expression level.

molecular modules. Further studies of their functions could increase our understanding of cambial differentiation during tree growth.

Differential expression of genes related to auxin distribution during vascular development

Auxin plays a critical role in regulating vascular development. Auxin accumulation and distribution are affected by genes en-

coding auxin transporters from the AUXIN1/LIKE-AUX1 (AUX/LAX), PIN-FORMED (PIN), and P-GLYCOPROTEIN/ATP-BINDING CASSETTE B4 (PGP/ABCB) families (Geisler et al., 2005; Petrásek et al., 2006; Cho et al., 2007). We examined the expression of various genes from these families in the scRNA-seq data to investigate the connection between auxin transporters and cambium differentiation and division in the *Populus* stem. Both the cell differentiation trajectories in PGT and SGT and the expression of auxin transporter genes,

**Figure 7. Fiber development analysis.**

- (A) UMAP analysis showing that the fiber cell cluster is separated into four subgroups. The subgroups are color coded.
- (B) Heatmap depicting the highly enriched genes in each fiber subgroup. Two columns list representative genes. Genes with known and unknown functions in fiber development are listed separately. The color of the dots indicates the expression level.
- (C) GO enrichment of the most enriched genes in each fiber subgroup.
- (D) Spatial expression pattern of fiber-enriched genes in the stem cross-section. The dot color indicates the expression level.

including *AUX1a/b/c*, *LAX2a*, *LAX3a/b*, *PIN6b*, and *PIN3a/b*, were examined (Figure 5; supplemental Figure 2). *LAX3a* was significantly expressed in the cambium throughout the pseudo-time differentiation trajectory, and its expression decreased as the cambium differentiated into xylem or phloem precursors in PGT and SGT (Figure 5). PGT and SGT also showed enhanced *LAX2a* and *AUX1b* expression as xylem identity was established (Figure 5). As xylem precursors differentiated,

AUX1c expression increased in SGT but remained unchanged in PGT (Figure 5). When phloem identity was established, expression of *PIN3a/b* and *LAX3b* increased in PGT (Figure 5A) but not in SGT (Figure 5B). Differentiation did not cause dynamic changes in *PIN6* or *AUX1a* in PGT or SGT (supplemental Figure 2A). Spatial transcriptome localization revealed that auxin transporters were expressed in various regions of the stem cross-section (supplemental Figure 2A).

PIN6, *PIN3*, *AUX1*, *LAX2*, and *LAX3* were all expressed in the cambium region (cambium, phloem, and xylem precursor cells), whereas *LAX2a*, *AUX1b*, and *AUX1c* were expressed mainly at xylem cell sites (supplemental Figure 2B). These findings suggest that auxin accumulation and distribution during cambium differentiation may be controlled by several auxin transporters, some of which may differ between PGT and SGT.

Molecular components of SCW thickening in fibers and vessels

SCW thickening is the basic process of wood formation. Different transcriptional networks are thought to control SCW biosynthesis in various cell types of wood tissue (Zhu and Li, 2021; Luo and Li, 2022). However, the specific transcriptional activity that controls SCW thickening in different cell types has yet to be established. Analysis of scRNA-seq data from developing wood revealed a number of potential markers for SCW formation in fibers and vessels (supplemental Figure 5A and 5B). Several genes encoding SCW biosynthesis enzymes exhibited a cell-type preference or specificity. For example, *IRREGULAR XYLEM 14* (*IRX14a*) xylan biosynthesis genes were found only in fibers (supplemental Figure 5A), whereas *PHENYLALANINE AMMONIA LYASE 1* (*PAL1a*) lignin biosynthesis-related genes were found only in vessels (supplemental Figure 5A). *LAC17* has four homologs in *Populus*; *LAC17a* and *LAC17d* were expressed primarily in vessel cells, and *LAC17c* was expressed only in fiber cells (supplemental Figure 5A and 5B). Numerous SCW synthesis enzymes were expressed in both fibers and vessels without regard for cell type (supplemental Figure 5C). These data imply that SCW biosynthesis may be regulated differently in different cell types. *ROPGAP3*, *PLANT GLYCOGENIN-LIKE STARCH INITIATION PROTEIN 5* (*PGSIP1*), and *PLASMODESMATA-LOCATED PROTEIN 6* (*PDLP6*) were specifically expressed in fibers (supplemental Figure 5A), whereas *GERMIN-LIKE PROTEIN 7* (*GLP7*) and *PIP2* were specifically expressed in vessels (supplemental Figure 5B). The particular cell-type preference of these genes has also been observed in other *Populus* scRNA-seq studies (supplemental Figure 6A–6F) (Li et al., 2021; Tung et al., 2023). Although the cell-type specificity of genes must be confirmed through further cellular studies, identification of new cell-type markers would be useful for obtaining novel insights into specific cell-wall biosynthesis in xylem and phloem.

We next analyzed the cell subpopulations in this study. We began by extracting vessel and fiber clusters. A combination of mutual nearest neighbors (Haghverdi et al., 2018) and canonical correlation analysis (Butler et al., 2018) methods in the Seurat package (v4.1.3) (Satija et al., 2015) was used for cell integration. The Clustree package was used to examine cluster changes under various resolution options. Highly enriched genes in subgroups were examined at several resolutions, and the resolution with the clearest association between gene expression and recognized developmental processes was chosen for subgroup analysis. There were four subgroups in the cell cluster designated as vessels (V1, V2, V3, and V4) (Figure 6A), and substantially enriched genes in each subgroup corresponded to the four successive stages of vessel development (Figure 6B; supplemental Table 8). Expression of

Molecular maps of cambium differentiation

WOX4, *ACL5*, *TRANSLOCASE OF THE OUTER MITOCHONDRIAL MEMBRANE 6* (*TOM6*), and other markers for cambium and xylem precursor cells revealed that the V1 subgroup retained these traits (Figure 6B). In V2, the xylem precursor genes *ACL5* and *AUX1* were expressed, but the cambium gene *WOX4* was not (Figure 6B). At the same time, expression of the transcription factor *MYB46*, a crucial regulator for SCW formation, started the thickening of SCWs in the vessels (Figure 6B). Prior to SCW thickening, the *EXPANSIN* (*EXPA*) and *XYLOGLUCAN ENDOTRANSGLUCOSYLASE* (*XTH*) family of genes, which is also expressed in V2, is needed to relax the cell wall (Figure 6B). GO analysis revealed that enriched genes at this stage had functional annotations for cell wall organization and cellular glucan metabolic pathway (Figure 6B and 6C). In V3, the SCW biosynthesis regulators *MYB42c* and *MYB52e* and genes encoding SCW biosynthesis enzymes, such as SCW-associated *CELLULOSE SYNTHASE 8* (*CESA8a*) and the lignin biosynthesis-related genes *PAL1c* and *4-COUMARATE:COA LIGASE 1* (*4CL1a*), were expressed (Figure 6B). Expression of these genes was reflected in GO functional annotations such as plant-type SCW biogenesis and lignin catabolic process (Figure 6C). In V4, SCW formation genes were continuously expressed, together with genes related to normal programmed cell death, such as *XCP1a* and *XCP2a/b* (Figure 6B). In addition to genes with known functions in vessel development, genes from the *BASIC HELIX-LOOP-HELIX* (*bHLH*), *BEL1-LIKE HOMEOBOX* (*BLH*), *ETHYLENE RESPONSE FACTOR* (*ERF*), *ARABIDOPSIS NAC DOMAIN-CONTAINING PROTEIN* (*ANAC*), *LBD*, *NITRATE TRANSPORTER* (*NPF*), and short peptide *RAPID ALKALINIZATION FACTOR* (*RALF*) families were also discovered (Figure 6B) and may represent new vessel regulators. *BHLH106b*, *ERF105b*, and *NRT1.1* were highly enriched in the V1 subgroup (Figure 6B); *BHLH145b*, *ERF003b*, and *NPF4.4a* in the V2 subgroup (Figure 6B); *BLH1b*, *ERF109c*, and *NPF5.2a* in the V3 subgroup (Figure 6B); and *BHLH128b*, *ERF110b*, and *NPF5.2a* in the V4 subgroup (Figure 6B). In addition, V3 and V4 expressed *ANAC087b*, which is involved in regulating the onset of cell death (Huysmans et al., 2018). This expression was corroborated by the spatial transcription location (Figure 6B and 6D).

Four subgroups were identified in the fiber cell cluster, and enriched genes in each subgroup corresponded to four successive developmental stages (Figure 7A; supplemental Table 9). Three (F1, F2, and F4) appeared to correspond with the progression of fiber development, but subgroup F3 did not clearly demonstrate a link with developmental phases (Figure 7B). Cells in the F1 subgroup expressed the xylem precursor genes *PHBa* and *KNAT7*, as well as the SCW formation regulators *MYB46b* and *MYB83*, indicating that SCW development had begun in this subgroup (Figure 7B). Expression of the SCW biosynthesis-regulating transcription factors *MYB52c/e* and the enzyme genes *CESA7b*, *LAC17c*, and *4CL1a* was enriched in the F2 subgroup (Figure 7B). More SCW synthesis enzyme genes, particularly those involved in lignin production such as *PAL1b*, *4CLa*, and *LAC17b*, and more transcription factors regulating SCW synthesis, including *SND2b/d*, *MYB52b*, and *MYB85*, were significantly enriched in the F4 subgroup (Figure 7B). GO functional annotations for plant-type SCW biogenesis also indicated the status of F2 and F4 (Figure 7C).

These findings suggested that fiber-related genes act sequentially in fiber formation. In addition, we discovered several transcription factors and genes involved in signal transduction that may be recognized as new candidate regulators in fiber formation. These included *RALFL33a/b/c*, *BLH3*, *BHLH62d*, and *ROP-GEF7b* in F1; *BLH7a*, *BHLH147a*, and *ROPGAP3b* in F2; and *BSK1a* and *TORTIFOLIA 1 (TOR1b)* in F4 (Figure 7C). Fibers selectively expressed *TOR1b*, which regulates microtubule-dependent cell elongation (Furutani et al., 2000) (Figure 7B). *BLH3*, which controls the timing of the vegetative-to-reproductive phase transition (Zhang et al., 2016), was found in the F1 subgroup (Figure 7B). The ROP activator gene *ROP (RHO OF PLANTS) GUANINE NUCLEOTIDE EXCHANGE FACTOR 7 (ROPGEF7b)*, which is involved in determining the metaxylem vessel pit pattern (Nagashima et al., 2018), was particularly upregulated in the F1 subgroup (Figure 7B). Spatial transcriptomics revealed where these genes were expressed on the stem cross-section (Figure 7D). By contrast, F3 lacked expression of any known xylem marker genes, and its enriched GO pathways did not involve cell wall organization or SCW biogenesis (Figure 7C). However, the F3 subgroup had a greater number of genes that were associated with reactions to heat, stress, and reactive oxygen (Figure 7C), and this subgroup overlapped with the other three subgroups in the UMAP graphic (Figure 7A). The F3 subgroup cells were grouped together within the fiber cells, but they exhibited numerous fiber-cell-specific traits. To understand how the subgroup cells are incorporated in subsequent SCW thickening, more research would be highly worthwhile.

DISCUSSION

The majority of the carbon fixed during photosynthesis in trees is converted and stored in their secondary xylem to produce wood, an essential and renewable biomaterial for human needs. Despite thorough descriptions of wood cell organization and structure in trees (Larson, 2012), we lack a thorough understanding of how cells differentiate to form wood. Here, we attempted to describe cellular atlases and regulatory networks of wood formation by building and comparing cell developmental trajectories in wood-forming tissues of *Populus*. The findings provide fresh insight into the processes of cellular differentiation during tree stem growth.

Single-cell transcriptomics of *Populus* stem development

The recent invention of scRNA-seq has revolutionized our understanding of transcriptional activity within tissues. However, few scRNA-seq experiments have been performed in plants, and the majority of these studies have used herbaceous *Arabidopsis* tissues. Spatial transcriptome sequencing has been used in animal studies, but it has only recently been applied to the study of plants (Liu et al., 2022; Xia et al., 2022). Perennial trees are distinguished by cambium proliferation and stem growth differentiation. Tree stem growth is supported by two cambium meristems, one in the shoot tip and the other in the vascular cambium ring. Similar and unique characteristics in cell identification and differentiation can be found in both meristem tissues (Baucher et al., 2007; Campbell and Turner, 2017).

We acquired scRNA transcriptome datasets from primary and secondary growth tissues. Identification of cell clusters and cell development were cross-verified by comparing the two datasets and spatial transcriptome data. Twelve cell clusters were identified in both PGT and SGT by linear dimensional reduction and resolution parameter optimization. Cell-type markers for cambium, xylem precursor, phloem precursor, sieve, and vessel cells were found in cell clusters of both PGT and SGT. Markers for phloem parenchyma and fiber cells were found only in SGT cell clusters, and markers for epidermis, cortex, and pith cells were found only in PGT cell clusters. Through spatial transcriptome analysis, expression of marker genes could be localized to appropriate cells in stem cross-sections. Three cell clusters in PGT and four in SGT could not be classified into their relevant cell types owing to the absence of suitable markers. These results suggested that there were both similarities and differences in cell arrangement between primary and secondary growth. scRNA transcriptomes revealed the expression of approximately 27 000 genes in PGT and 29 317 genes in SGT; however, the expression of genes abundant in cell clusters varied between PGT and SGT. Comparison of scRNA transcriptome datasets from the two tissues could facilitate identification of essential regulators in the two developmental stages.

Transcriptional control of cambium differentiation

In secondary growth, cell differentiation after cambium proliferation is essential for expansion of stem diameter. Studies have shown that a complex network of transcriptional programs and hormone signals regulates differentiation (Ye and Zhong, 2015; Luo and Li, 2022). The majority of these studies have focused on tissue-level molecular dissection, and it remains unknown how differentiation is dynamically and sequentially regulated at the cellular level. Here, construction of pseudo-time trajectories revealed that branch-determining genes control cambium differentiation in two directions: toward xylem and phloem. The auxin transporters *AUX1b*, *LAX2*, *IAA9*, *IAA11a*, *IAA13a/b*, and *IAA19a/b* were dynamically expressed in the differentiation trajectory toward xylem in both PGT and SGT, suggesting that auxin signaling and distribution are crucial for xylem differentiation. Impaired xylem differentiation in *aux1/lax1/lax2/lax3* mutants of *Arabidopsis* supports this conclusion (Fabregas et al., 2015). Auxin distribution shows a peak in the vascular cambium of *Populus* (Immanen et al., 2016), and the VCM1-PIN5 molecular module controls auxin concentration to control xylem differentiation (Zheng et al., 2021). Dynamic regulation of auxin distribution during xylem development is implied by the involvement of distinct auxin transporters in differentiation. However, more research is needed to understand the genetic processes by which auxin transporters contribute to secondary growth in trees.

In addition to auxin-associated genes, we discovered other transporters, including the SWEET sugar transporters *SWEET1a*, *SWEET17a*, and *SWEET2a*. A recent *Arabidopsis* study showed that the *sweet16* mutant has fewer xylem cells and that *SWEET16* is expressed at the procambium–xylem interface (Aubry et al., 2022). Furthermore, overexpression of *SWEET7* in *Populus* promotes xylem growth (Zhang et al., 2021). All of these findings suggest that sugar transport influences cambium differentiation. The trajectory also revealed the presence of two small peptide genes, *RALFL33a/b* and *RALFL34a/b*. They

appear to function as a signal in cambium differentiation. A large number of transcription factor genes also showed branch-dependent expression during differentiation. As potential new regulatory factors, these genes may participate in the regulation of cambial differentiation.

The xylem is mainly composed of two cell types with thickened SCWs: vessel cells for mineral and water transport and fiber cells for mechanical support. These are also the main cell components for biomaterial production (Ek et al., 2009; Gorshkova et al., 2012). Although both cell types go through comparable developmental processes, such as cell expansion, secondary wall thickening, and programmed cell death, their secondary wall thickening may be controlled by different transcriptional regulatory networks (Ye and Zhong, 2015; Zhu and Li, 2021). In this work, we examined the developmental trajectories of fiber and vessel cells. Some functional genes were shared across fiber and vessel cells, but others were cell specific, such as four homologs of the laccase gene *LAC17*, which functions in lignin synthesis. Several transcription factors and signaling molecules were also expressed at different developmental stages of the two cell types, suggesting that they may have regulatory roles in the development of fiber and vessel cells. Overall, these findings contribute to a better understanding of the molecular regulatory networks involved in the formation of fiber and vessel cells and provide a basis for future wood modification via cell-specific mechanisms.

Understanding the growth of tree stems via cellular transcriptomes

Tree stem growth is caused by proliferation of the vascular cambium, followed by cellular differentiation, and this is the primary pathway for storage of photosynthetically fixed carbon in lignocellulosic biomass in trees (Pan et al., 2011). The use of scRNA-seq analysis allows for a cellular-level description of the molecular activity of a tissue, and analysis of single-cell transcriptomes in *Populus* stem tissues has recently been described (Chen et al., 2021; Li et al., 2021; Tung et al., 2023). These scRNA-seq experiments focused on xylem tissue cells. However, because a limited number of marker genes are available for cell-type identification in growing stem tissue, cell clusters identified in scRNA-seq datasets could not be unambiguously assigned to specific cell types. This limitation results from a lack of understanding of how trees grow. To investigate cambium differentiation in various directions, we collected cells from both sides of the cambium in growing stem tissues. We were able to cross-check the cambium differentiation trajectories by comparing primary and secondary stem tissues at the same time. A large number of genes have been identified as participating in the process of cell differentiation during stem cell proliferation using scRNA-seq research. However, further experimental characterization is required to properly characterize their functional mechanisms in cambium differentiation and xylem development. Spatial transcriptome analysis, on the other hand, enables observation of cellular transcriptomes *in situ*. However, owing to its restricted resolution when applied to plant tissues, spatial transcriptome analysis in plants is still in its early stages. The combination of scRNA-seq with spatial transcriptome analysis therefore provides a systematic view of the molecular networks involved in wood formation at the cellular level.

METHODS

Tree growth conditions and protoplast isolation

A phytotron was used to cultivate *Populus euramericana* cv. 'Nanlin895' for 2 months under a 16-h light/8-h dark photoperiod. Intact protoplasts were isolated according to a previously described procedure with some modifications (Lin et al., 2014). To obtain single-cell transcriptomes, the first to third internodes were extracted as PGT and the fifth to tenth internodes as SGT. Internodes from the sampled plants were divided into outer bark and inner woody tissue, then immersed in a solution for breaking down cell walls that contained 1.5% (wt/vol) cellulase R-10, 0.4% (wt/vol) macerozyme R-10, 0.6 M mannitol, 20 mM KCl, 10 mM CaCl₂, and 0.1% (wt/vol) bovine serum albumin. After vacuum extraction and lysis in the dark for 2 h, protoplasts were collected by centrifuging twice at 300 g for 3 min. This step removed any clumped cells. Protoplasts were resuspended in a 0.6 M mannitol solution. After centrifuging at 700 g for 1 min, 1 mL of the resuspension was added to 5 mL of a 2 M sucrose solution. Trypan blue staining was used to check protoplast concentration and viability. Protoplasts with a viability rating of >75% were used immediately for single-cell sequencing analysis.

scRNA-seq library construction and sequencing

As directed by the vendor, scRNA-seq libraries were created using the 10x Chromium Single Cell 3' Platform (10x Genomics, Pleasanton, CA). To create single-cell GEMs, protoplasts were briefly injected onto a chromium microfluidic chip (gel beads in emulsion). The Chromium Single Cell 3' library kit v3.1 was used to create scRNA-seq libraries (10x Genomics). An Agilent 2100 Bioanalyzer was used to analyze the libraries, and the Illumina NovaSeq 6000 platform was used to sequence the data.

Spatial transcriptome library construction and sequencing

The fourth internode was obtained from a 2-month-old *Populus* tree, embedded in optimal cutting temperature compound, and cryosectioned. Hematoxylin and eosin was used to stain the sections. A cDNA library was constructed on the 10x Visium platform according to the manufacturer's instructions, and the DNBSEQ-T7 platform was used for sequencing.

Cell clustering and scRNA-seq data analysis

The *Populus trichocarpa* v4.1 genome was used to align the raw scRNA-seq data. Cell Ranger algorithms produced expression matrices for every gene and every cell. Additional analysis was performed using Seurat software (v4.1.3) (Satija et al., 2015). Doublets (two or more cells in a single oil droplet) were removed using DoubletFinder (v4.1.2) (McGinnis et al., 2019). A gene was counted if it was expressed in at least three distinct cells. Cells that expressed more than 10 000 genes, fewer than 500 genes, or more than 5% mitochondrial genes were eliminated. In the data matrix, this method produced 7416 and 11 769 cells from PGT and SGT, respectively. We used canonical correlation analysis and mutual closest neighbors approaches in Seurat software (v4.1.3) for integration of vascular cells. The remaining matrix was then normalized in Seurat (v4.1.3) via LogNormalize. FindVariableFeatures with the selection.method = "vst" option was used to identify highly variable genes, and the top 2000 genes were used for PCA to reduce the linear dimensionality. Clustree (v0.4.4) was used to determine the ideal resolution parameter for cluster identification. Using the Seurat function FindClusters with resolution = 0.3, the first 20 PCs were used to find cell clusters, which were then visualized and investigated with UMAP (Becht et al., 2018). FindAllMarkers was implemented in Seurat (v4.1.3) with the settings "min.pct = 0.25" and "logfc.threshold = 0.58" to identify cluster-enriched genes (Satija et al., 2015).

Analysis of spatial transcriptome data and cell clustering

The *Populus trichocarpa* v4.1 genome was used to align the raw scRNA-seq data. Expression matrices for each gene and each location were created using Visium Ranger algorithms. Further analysis was performed with Seurat software (v4.1.3) (Satija et al., 2015). In Seurat (v4.1.3), the

matrix was normalized using SCTransform. PCA was used to reduce linear dimensionality. Using the Seurat function FindClusters with “resolution = 0.5”, the first 30 PCs were used to find cell clusters, which were then visualized and investigated with UMAP (Becht et al., 2018). FindAllMarkers was implemented in Seurat (v4.1.3) with the settings “min.pct = 0.25” and “logfc.threshold = 0.58” to identify cluster-enriched genes.

Pseudo-time analysis

A continuous developmental trajectory was created using the R program Monocle2 (v4.1.1) (Qiu et al., 2017). In brief, the cluster-enriched genes were used to select and arrange the cells of interest. The data were split into two components using the DDRTree approach, and branch-dependent genes were identified using BEAM.

Pathway analysis

The R package clusterProfiler (v4.1.2) was used for pathway enrichment analysis (Yu et al., 2012). The pvalueCutoff, qvalueCutoff, and pAdjustMethod parameters were set to 0.01, 0.05, and BH, respectively.

Gene information

Supplemental Table 10 provides JGI numbers and other information for all genes mentioned in this study.

In situ hybridization

In situ hybridization was performed according to a previously published method (Dai et al., 2023). In brief, *Populus* stems were fixed with FAA (formalin-aceto-alcohol), dehydrated in an alcohol gradient, infiltrated with paraffin, and finally embedded in paraffin. A gene-specific segment of 100–150 bp was selected and amplified by PCR (primers used are listed in supplemental Table 11), then assembled into the intermediate vector, transcribed *in vitro*, and labeled with digoxin according to the manufacturer’s instructions (Roche 10999644001; Roche 3359247910). Sections were fixed on poly-lysine slides. After pretreatment, probes were hybridized with sections overnight at 48°C, after which antibodies were incubated for the final color reaction.

DATA AND CODE AVAILABILITY

The raw sequence data reported in this paper have been deposited in the Genome Sequence Archive at the National Genomics Data Center, China National Center for Bioinformation/Beijing Institute of Genomics, Chinese Academy of Sciences (GSA: CRA010013) and are publicly accessible at <https://ngdc.cncb.ac.cn/gsa>.

SUPPLEMENTAL INFORMATION

Supplemental information is available at *Plant Communications Online*.

FUNDING

This research was supported by the National Natural Science Foundation of China (32130072), the Chinese Academy of Sciences’ Strategic Priority Research Program (XDB27020104), and the National Key Research and Development Program (2021YFD2200204).

AUTHOR CONTRIBUTIONS

L.L. conceived the project. J.W. made suggestions for the project. R.L. and Z.W. performed the experiments. R.L. and L.L. analyzed the data and wrote the manuscript. All authors discussed the results and approved the final manuscript.

ACKNOWLEDGMENTS

We thank Dr. Tianqi Zhang from the CAS Center for Excellence in Molecular Plant Sciences for assisting with the construction of the single-cell RNA library, as well as Drs. Quanzi Li from the Chinese Academy of Forestry, Tao Ma from Sichuan University, and Ying-Chung Jimmy Lin from National Taiwan University for sharing the single-cell sequencing data. No conflict of interest is declared.

Received: February 27, 2023

Revised: July 4, 2023

Accepted: July 24, 2023

Published: July 24, 2023

REFERENCES

- Aubry, E., Hoffmann, B., Vilaine, F., Gilard, F., Klemens, P.A., Guérard, F., Gakière, B., Neuhaus, H.E., Bellini, C., and Dinant, S. (2022). A vacuolar hexose transport is required for xylem development in the inflorescence stem. *Plant Physiol.* **188**:1229–1247.
- Avcı, U., Earl Petzold, H., Ismail, I.O., Beers, E.P., and Haigler, C.H. (2008). Cysteine proteases XCP1 and XCP2 aid micro-autolysis within the intact central vacuole during xylogenesis in *Arabidopsis* roots. *Plant J.* **56**:303–315. <https://doi.org/10.1111/j.1365-313X.2008.03592.x>.
- Barratt, D.H.P., Kölling, K., Graf, A., Pike, M., Calder, G., Findlay, K., Zeeman, S.C., and Smith, A.M. (2011). Callose synthase GSL7 is necessary for normal phloem transport and inflorescence growth in *Arabidopsis*. *Plant Physiol.* **155**:328–341. <https://doi.org/10.1104/pp.110.166330>.
- Baucher, M., El Jaziri, M., and Vandepitte, O. (2007). From primary to secondary growth: origin and development of the vascular system. *J. Exp. Bot.* **58**:3485–3501.
- Becht, E., McInnes, L., Healy, J., Dutertre, C.A., Kwok, I.W.H., Ng, L.G., Ginhoux, F., and Newell, E.W. (2018). Dimensionality reduction for visualizing single-cell data using UMAP. *Nat. Biotechnol.* **37**:38–44. <https://doi.org/10.1038/nbt.4314>.
- Bonke, M., Thitamadee, S., Mähönen, A.P., Hauser, M.T., and Helariutta, Y. (2003). APL regulates vascular tissue identity in *Arabidopsis*. *Nature* **426**:181–186. <https://doi.org/10.1038/nature02100>.
- Bossinger, G., and Spokevicius, A.V. (2018). Sector analysis reveals patterns of cambium differentiation in poplar stems. *J. Exp. Bot.* **69**:4339–4348.
- Butler, A., Hoffman, P., Smibert, P., Papalexi, E., and Satija, R. (2018). Integrating single-cell transcriptomic data across different conditions, technologies, and species. *Nat. Biotechnol.* **36**:411–420. <https://doi.org/10.1038/nbt.4096>.
- Campbell, L., and Turner, S. (2017). Regulation of vascular cell division. *J. Exp. Bot.* **68**:27–43.
- Carlquist, S. (2013). Comparative Wood Anatomy: Systematic, Ecological, and Evolutionary Aspects of Dicotyledon Wood (Springer Science & Business Media).
- Chen, Y., Tong, S., Jiang, Y., Ai, F., Feng, Y., Zhang, J., Gong, J., Qin, J., Zhang, Y., Zhu, Y., et al. (2021). Transcriptional landscape of highly lignified poplar stems at single-cell resolution. *Genome Biol.* **22**:319. <https://doi.org/10.1186/s13059-021-02537-2>.
- Cho, M., Lee, S.H., and Cho, H.-T. (2007). P-Glycoprotein4 displays auxin efflux transporter-like action in *Arabidopsis* root hair cells and tobacco cells. *Plant Cell* **19**:3930–3943.
- Clay, N.K., and Nelson, T. (2005). *Arabidopsis* thickvein mutation affects vein thickness and organ vascularization, and resides in a provascular cell-specific spermine synthase involved in vein definition and in polar auxin transport. *Plant Physiol.* **138**:767–777. <https://doi.org/10.1104/pp.104.055756>.
- Dai, X., Zhai, R., Lin, J., Wang, Z., Meng, D., Li, M., Mao, Y., Gao, B., Ma, H., Zhang, B., et al. (2023). Cell-type-specific PtrWOX4a and PtrVCS2 form a regulatory nexus with a histone modification system for stem cambium development in *Populus trichocarpa*. *Nat. Plants* **9**:96–111. <https://doi.org/10.1038/s41477-022-01315-7>.
- Depuydt, S., Rodriguez-Villalon, A., Santuari, L., Wyser-Rmili, C., Ragni, L., and Hardtke, C.S. (2013). Suppression of *Arabidopsis* protophloem differentiation and root meristem growth by CLE45

Plant Communications

- requires the receptor-like kinase BAM3. Proc. Natl. Acad. Sci. USA **110**:7074–7079. <https://doi.org/10.1073/pnas.1222314110>.
- Ek, M., Gellerstedt, G., and Henriksson, G.** (2009). *Wood Chemistry and Wood Biotechnology* (Walter de Gruyter).
- Esau, K.** (1977). *Anatomy of Seed Plants* (John Wiley and Sons).
- Fabregas, N., Formosa-Jordan, P., Confraria, A., Siligato, R., Alonso, J.M., Swarup, R., Bennett, M.J., Mahonen, A.P., Cano-Delgado, A.I., and Ibanes, M.** (2015). Auxin Influx Carriers Control Vascular Patterning and Xylem Differentiation in *Arabidopsis thaliana*. *PLoS Genet.* **11**. <https://doi.org/10.1371/journal.pgen.1005183>.
- Funk, V., Kositsup, B., Zhao, C., and Beers, E.P.** (2002). The *Arabidopsis* Xylem Peptidase XCP1 Is a Tracheary Element Vacuolar Protein That May Be a Papain Ortholog. *Plant Physiol.* **128**:84–94. <https://doi.org/10.1104/pp.010514>.
- Geisler, M., Blakeslee, J.J., Bouchard, R., Lee, O.R., Vincenzetti, V., Bandyopadhyay, A., Titapiwatanakun, B., Peer, W.A., Bailly, A., Richards, E.L., et al.** (2005). Cellular efflux of auxin catalyzed by the *Arabidopsis* MDR/PGP transporter AtPGP1. *Plant J.* **44**:179–194.
- Gorshkova, T., Brutch, N., Chabbert, B., Deyholos, M., Hayashi, T., Lev-Yadun, S., Mellerowicz, E.J., Morvan, C., Neutelings, G., and Pilate, G.** (2012). Plant fiber formation: state of the art, recent and expected progress, and open questions. *Crit. Rev. Plant Sci.* **31**:201–228.
- Haghverdi, L., Lun, A.T.L., Morgan, M.D., and Marioni, J.C.** (2018). Batch effects in single-cell RNA-seqencing data are corrected by matching mutual nearest neighbors. *Nat. Biotechnol.* **36**:421–427. <https://doi.org/10.1038/nbt.4091>.
- Huysmans, M., Buono, R.A., Skorzinski, N., Radio, M.C., De Winter, F., Parizot, B., Mertens, J., Karimi, M., Fendrych, M., and Nowack, M.K.** (2018). NAC transcription factors ANAC087 and ANAC046 control distinct aspects of programmed cell death in the *Arabidopsis* columella and lateral root cap. *Plant Cell* **30**:2197–2213.
- Furutani, I., Watanabe, Y., Prieto, R., Masukawa, M., Suzuki, K., Naoi, K., Thitamadee, S., Shikanai, T., and Hashimoto, T.** (2000). The SPIRAL genes are required for directional control of cell elongation in *Arabidopsis thaliana*. *Development* **127**:4443–4453.
- Immanen, J., Nieminen, K., Smolander, O.-P., Kojima, M., Alonso Serra, J., Koskinen, P., Zhang, J., Elo, A., Mähönen, A.P., Street, N., et al.** (2016). Cytokinin and auxin display distinct but interconnected distribution and signaling profiles to stimulate cambial activity. *Curr. Biol.* **26**:1990–1997.
- Kim, J.-Y., Symeonidi, E., Pang, T.Y., Denyer, T., Weidauer, D., Bezrutczyk, M., Miras, M., Zöllner, N., Hartwig, T., Wudick, M.M., et al.** (2021). Distinct identities of leaf phloem cells revealed by single cell transcriptomics. *Plant Cell* **33**:511–530.
- Kuroha, T., Tokunaga, H., Kojima, M., Ueda, N., Ishida, T., Nagawa, S., Fukuda, H., Sugimoto, K., and Sakakibara, H.** (2009). Functional analyses of LONELY GUY cytokinin-activating enzymes reveal the importance of the direct activation pathway in *Arabidopsis*. *Plant Cell* **21**:3152–3169. <https://doi.org/10.1105/tpc.109.068676>.
- Larson, P.R.** (2012). *The Vascular Cambium: Development and Structure* (Springer Science & Business Media).
- Li, H., Dai, X., Huang, X., Xu, M., Wang, Q., Yan, X., Sederoff, R.R., and Li, Q.** (2021). Single-cell RNA sequencing reveals a high-resolution cell atlas of xylem in *Populus*. *J. Integr. Plant Biol.* **63**:1906–1921. <https://doi.org/10.1111/jipb.13159>.
- Lin, Y.C., Li, W., Chen, H., Li, Q., Sun, Y.H., Shi, R., Lin, C.Y., Wang, J.P., Chen, H.C., Chuang, L., et al.** (2014). A simple improved-throughput xylem protoplast system for studying wood formation. *Nat. Protoc.* **9**:2194–2205. <https://doi.org/10.1038/nprot.2014.147>.
- Liu, C., Leng, J., Li, Y., Ge, T., Li, J., Chen, Y., Guo, C., and Qi, J.** (2022). A spatiotemporal atlas of organogenesis in the development of orchid flowers. *Nucleic Acids Res.* **50**:9724–9737. <https://doi.org/10.1093/nar/gkac773>.
- Luo, L., and Li, L.** (2022). Molecular understanding of wood formation in trees. *For. Res.* **2**:0. <https://doi.org/10.48130/FR-2022-0005>.
- McGinnis, C.S., Murrow, L.M., and Gartner, Z.J.** (2019). DoubletFinder: Doublet Detection in Single-Cell RNA Sequencing Data Using Artificial Nearest Neighbors. *Cell Syst.* **8**:329–337.e4. <https://doi.org/10.1016/j.cels.2019.03.003>.
- Muñiz, L., Minguet, E.G., Singh, S.K., Pesquet, E., Vera-Sirera, F., Moreau-Courtois, C.L., Carbonell, J., Blázquez, M.A., and Tuominen, H.** (2008). ACAULIS5 controls *Arabidopsis* xylem specification through the prevention of premature cell death. *Development* **135**:2573–2582.
- Nagashima, Y., Tsugawa, S., Mochizuki, A., Sasaki, T., Fukuda, H., and Oda, Y.** (2018). A Rho-based reaction-diffusion system governs cell wall patterning in metaxylem vessels. *Sci. Rep.* **8**:11542.
- Nieminen, K., Blomster, T., Helariutta, Y., and Mähönen, A.P.** (2015). Vascular cambium development. *The Arabidopsis Book/American Society of Plant Biologists* **13**:e0177.
- Pan, Y., Birdsey, R.A., Fang, J., Houghton, R., Kauppi, P.E., Kurz, W.A., Phillips, O.L., Shvidenko, A., Lewis, S.L., Canadell, J.G., et al.** (2011). A large and persistent carbon sink in the world's forests. *Science* **333**:988–993.
- Pélissier, H.C., Peters, W.S., Collier, R., van Bel, A.J.E., and Knoblauch, M.** (2008). GFP tagging of sieve element occlusion (SEO) proteins results in green fluorescent forisomes. *Plant Cell Physiol.* **49**:1699–1710. <https://doi.org/10.1093/pcp/pcn141>.
- Petrásek, J., Mravec, J., Bouchard, R., Blakeslee, J.J., Abas, M., Seifertová, D., Wisniewska, J., Tadele, Z., Kubes, M., Covánová, M., et al.** (2006). PIN proteins perform a rate-limiting function in cellular auxin efflux. *Science* **312**:914–918.
- Prassinos, C., Ko, J.-H., Yang, J., and Han, K.-H.** (2005). Transcriptome Profiling of Vertical Stem Segments Provides Insights into the Genetic Regulation of Secondary Growth in Hybrid Aspen Trees. *Plant Cell Physiol.* **46**:1213–1225. <https://doi.org/10.1093/pcp/pci130>.
- Prigge, M.J., Otsuga, D., Alonso, J.M., Ecker, J.R., Drews, G.N., and Clark, S.E.** (2005). Class III homeodomain-leucine zipper gene family members have overlapping, antagonistic, and distinct roles in *Arabidopsis* development. *Plant Cell* **17**:61–76. <https://doi.org/10.1105/tpc.104.026161>.
- Qiu, X., Mao, Q., Tang, Y., Wang, L., Chawla, R., Pliner, H.A., and Trapnell, C.** (2017). Reversed graph embedding resolves complex single-cell trajectories. *Nat. Methods* **14**:979–982. <https://doi.org/10.1038/nmeth.4402>.
- Rahimi, A., Karami, O., Lestari, A.D., de Werk, T., Amakorová, P., Shi, D., Novák, O., Greb, T., and Offringa, R.** (2022). Control of cambium initiation and activity in *Arabidopsis* by the transcriptional regulator AHL15. *Curr. Biol.* **32**:1764–1775.e3.
- Rodríguez-Villalon, A., Gujas, B., Kang, Y.H., Breda, A.S., Cattaneo, P., Depuydt, S., and Hardtke, C.S.** (2014). Molecular genetic framework for protophloem formation. *Proc. Natl. Acad. Sci. USA* **111**:11551–11556. <https://doi.org/10.1073/pnas.1407337111>.
- Satija, R., Farrell, J.A., Gennert, D., Schier, A.F., and Regev, A.** (2015). Spatial reconstruction of single-cell gene expression data. *Nat. Biotechnol.* **33**:495–502. <https://doi.org/10.1038/nbt.3192>.
- Suer, S., Agusti, J., Sanchez, P., Schwarz, M., and Greb, T.** (2011). WOX4 Imparts Auxin Responsiveness to Cambium Cells in *Arabidopsis*. *Plant Cell* **23**:3247–3259. <https://doi.org/10.1105/tpc.111.087874>.
- To, J.P.C., Derrière, J., Maxwell, B.B., Morris, V.F., Hutchison, C.E., Ferreira, F.J., Schaller, G.E., and Kieber, J.J.** (2007). Cytokinin regulates type-A *Arabidopsis* Response Regulator activity and

Molecular maps of cambium differentiation

- protein stability via two-component phosphorelay. *Plant Cell* **19**:3901–3914. <https://doi.org/10.1105/tpc.107.052662>.
- Tung, C.C., Kuo, S.C., Yang, C.L., Yu, J.H., Huang, C.E., Liou, P.C., Sun, Y.H., Shuai, P., Su, J.C., Ku, C., and Lin, Y.C.J.** (2023). Single-cell transcriptomics unveils xylem cell development and evolution. *Genome Biol.* **24**:3. <https://doi.org/10.1186/s13059-022-02845-1>.
- Vidaurre, D.P., Ploense, S., Krogan, N.T., and Berleth, T.** (2007). AMP1 and MP antagonistically regulate embryo and meristem development in Arabidopsis. *Development* **134**:2561–2567. <https://doi.org/10.1242/dev.006759>.
- Xia, K., Sun, H.-X., Li, J., Li, J., Zhao, Y., Chen, L., Qin, C., Chen, R., Chen, Z., Liu, G., et al.** (2022). The single-cell stereo-seq reveals region-specific cell subtypes and transcriptome profiling in Arabidopsis leaves. *Dev. Cell* **57**:1299–1310.e4. <https://doi.org/10.1016/j.devcel.2022.04.011>.
- Xie, B., Wang, X., Zhu, M., Zhang, Z., and Hong, Z.** (2011). CalS7 encodes a callose synthase responsible for callose deposition in the phloem. *Plant J.* **65**:1–14. <https://doi.org/10.1111/j.1365-313X.2010.04399.x>.
- Ye, Z.-H., and Zhong, R.** (2015). Molecular control of wood formation in trees. *J. Exp. Bot.* **66**:4119–4131.
- Yu, G., Wang, L.G., Han, Y., and He, Q.Y.** (2012). clusterProfiler: an R package for comparing biological themes among gene clusters. *OMICS* **16**:284–287. <https://doi.org/10.1089/omi.2011.0118>.
- Zhang, J., Eswaran, G., Alonso-Serra, J., Kucukoglu, M., Xiang, J., Yang, W., Elo, A., Nieminen, K., Damén, T., Joung, J.-G., et al.** (2019). Transcriptional regulatory framework for vascular cambium development in Arabidopsis roots. *Nat. Plants* **5**:1033–1042.
- Zhang, L., Wang, L., Zhang, J., Song, C., Li, Y., Li, J., and Lu, M.** (2021). Expression and localization of SWEETs in Populus and the effect of SWEET7 overexpression in secondary growth. *Tree Physiol.* **41**:882–899.
- Zhang, L., Zhang, X., Ju, H., Chen, J., Wang, S., Wang, H., Zhao, Y., and Chang, Y.** (2016). Ovate family protein1 interaction with BLH3 regulates transition timing from vegetative to reproductive phase in Arabidopsis. *Biochem. Biophys. Res. Commun.* **470**:492–497. <https://doi.org/10.1016/j.bbrc.2016.01.135>.
- Zhao, Y., Zhang, Q., Yuan, L., Zhang, R., and Li, L.** (2013). N-glycosylation and dimerization regulate the PtrMAN6 enzyme activity that may modulate generation of oligosaccharide signals. *Plant Signal. Behav.* **8**:e26956. <https://doi.org/10.4161/psb.26956>.
- Zheng, S., He, J., Lin, Z., Zhu, Y., Sun, J., and Li, L.** (2021). Two MADS-box genes regulate vascular cambium activity and secondary growth by modulating auxin homeostasis in Populus. *Plant Commun.* **2**:100134. <https://doi.org/10.1016/j.xplc.2020.100134>.
- Zhong, R., Lee, C., Zhou, J., McCarthy, R.L., and Ye, Z.H.** (2008). A battery of transcription factors involved in the regulation of secondary cell wall biosynthesis in Arabidopsis. *Plant Cell* **20**:2763–2782. <https://doi.org/10.1105/tpc.108.061325>.
- Zhong, R., Demura, T., and Ye, Z.H.** (2006). SND1, a NAC domain transcription factor, is a key regulator of secondary wall synthesis in fibers of Arabidopsis. *Plant Cell* **18**:3158–3170. <https://doi.org/10.1105/tpc.106.047399>.
- Zhou, J., Zhong, R., and Ye, Z.H.** (2014). Arabidopsis NAC domain proteins, VND1 to VND5, are transcriptional regulators of secondary wall biosynthesis in vessels. *PLoS One* **9**:e105726. <https://doi.org/10.1371/journal.pone.0105726>.
- Zhu, Y., and Li, L.** (2021). Multi-layered regulation of plant cell wall thickening. *Plant Cell Physiol.* **62**:1867–1873.
- Zhu, Y., Song, D., Xu, P., Sun, J., and Li, L.** (2018). A HD-ZIP III gene, PtrHB4, is required for interfascicular cambium development in Populus. *Plant Biotechnol. J.* **16**:808–817.